nature nanotechnology

SUPPLEMENTARY INFORMATION

DOI: 10.1038/NNANO.2009.81

**A. Additional SEM images, demonstrating that our assembly method is independent of the specific material or shape of the QDs, and readily scales from trenches down to 5 nm in width to much wider trenches.**

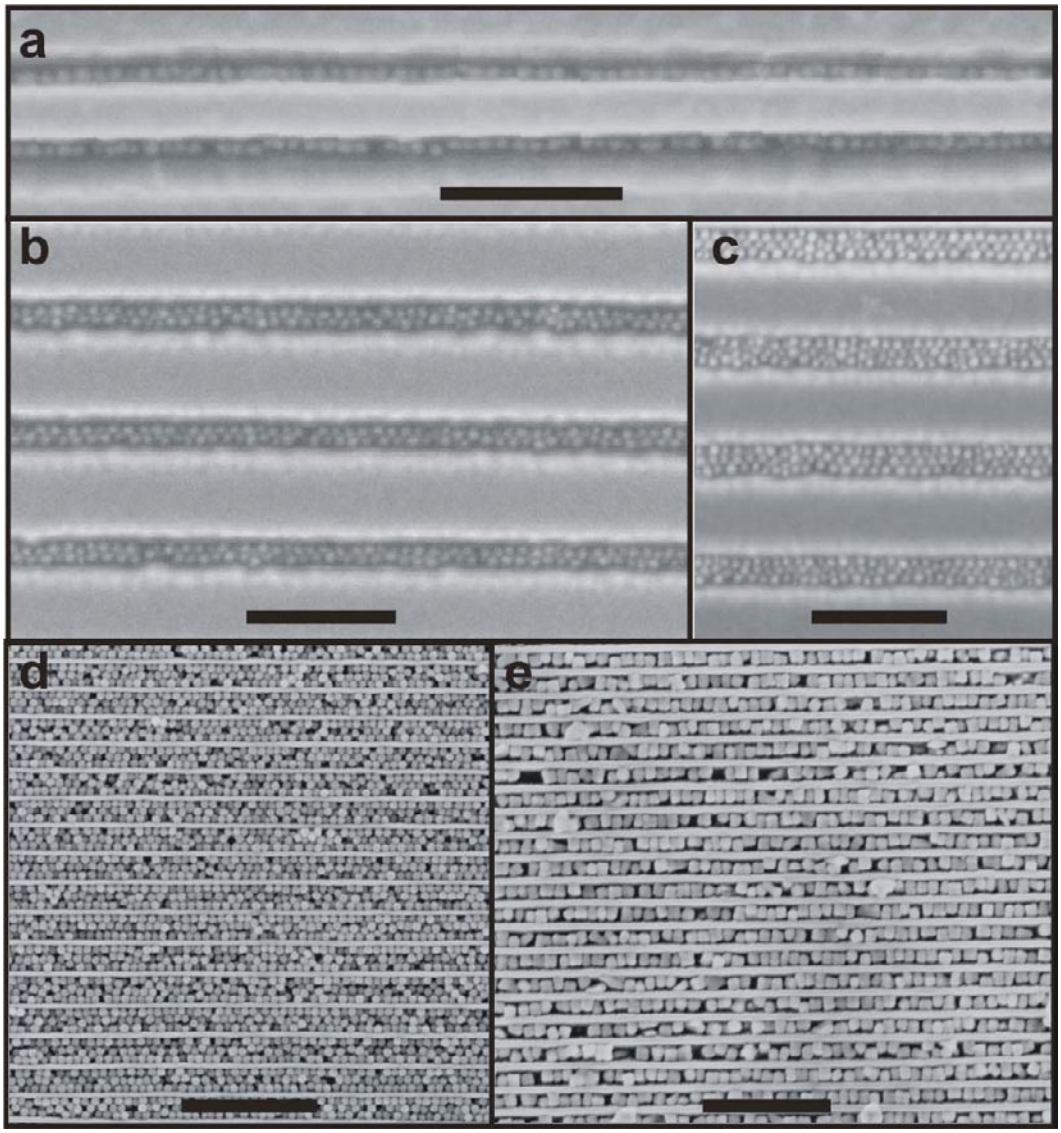


**Supplementary Figure 1. Additional SEM images.** SEM images of **(a)** 1-line, **(b)** 2-line, **(c)** 3-line arrays of 5 nm Au QDs. **(d)** 3-line arrays of 25 nm magnetite QDs. **(e)** 1-line arrays of 40 nm cuboid magnetite QDs. Scale bars: **(a), (b), (c),** 100 nm; **(d), (e),** 400 nm.

DOI: 10.1038/NNANO.2009.81

**B. Linear dependence of resistance per array on array length:**

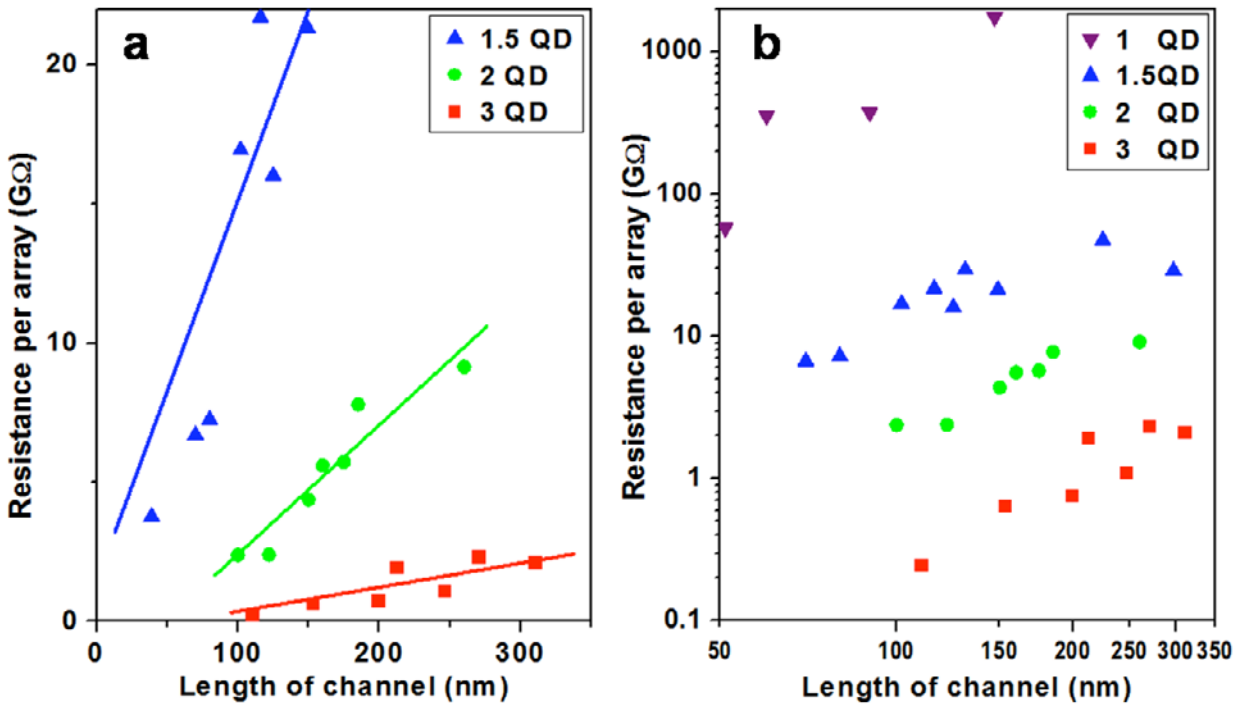


**Supplementary Figure 2. Measured resistance per array at room temperature as a function of array length for quasi-1D and 1D QD arrays with different widths. a**, Plotted on linear scales. **b**, Plotted on logarithmic scales. The number of QDs across the width of each array is label in the graph. 1D zigzag arrays are labeled as 1.5 QD.

We fabricated a number of devices, each contacting 50 to 400 parallel quasi-1D or 1D QD arrays, and plotted the measured resistance per array at room temperature as a function of array length (Supplementary Fig. 2). A clear linear dependence is observed, indicating that the transport properties of the devices are dominated by the QD arrays with negligible contribution from contacts. In addition, consistent trends are found for different arrangement of QD arrays: data from arrays with the same number of QDs across the width of each array follow the same linear trend, whereas much larger resistance per array is found as the number of QDs across is reduced, thus demonstrating the high level of control and reproducibility in our assembly.

## C. Temperature-dependent conductance data obtained on different 1D zigzag (1.5 QD) array devices

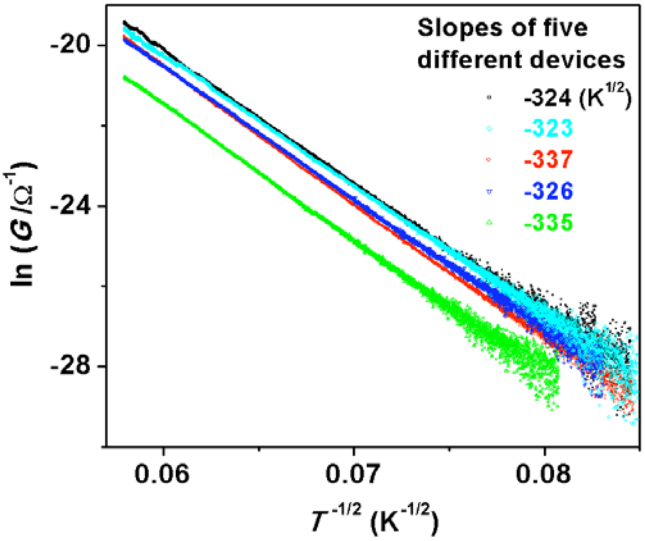


**Supplementary Figure 3. The temperature-dependent conductance data obtained on five different 1D zigzag (1.5 QD) array devices.** The slopes of each set of data are labeled in the graph.

For 1D zigzag (1.5 QD) arrays, we have performed temperature-dependent conductance measurement on five different devices and presented the obtained ln($G$)-$T^{-1/2}$ slopes in the inset of Fig. 2b, but only plotted three sets of the conductance data in Fig. 2b due to the overlapping between data obtained from different devices. The full dataset is re-plotted with different colors in Supplementary Fig. 3. Consistent results (in particular, the ln($G$)-$T^{-1/2}$ slopes, as labeled in the graph) are observed for different devices.

DOI: 10.1038/NNANO.2009.81

## D. Electrical properties of the 1D zigzag QD arrays at high voltage

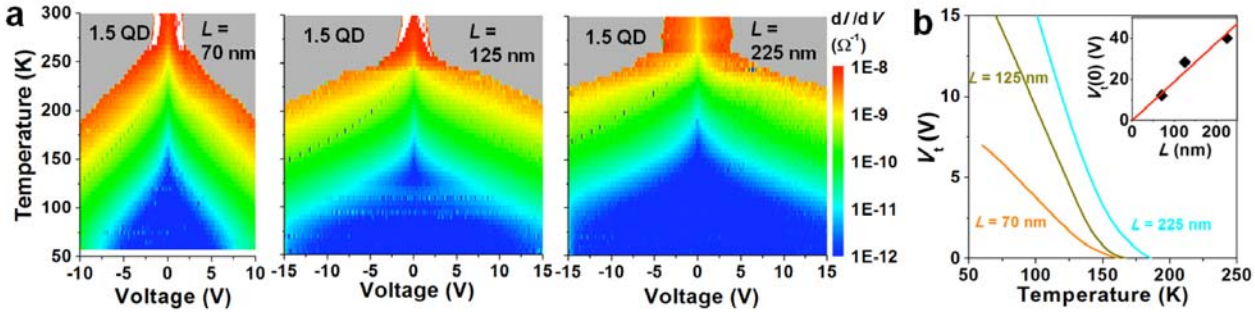


**Supplementary Figure 4. Electrical properties of the 1D zigzag QD arrays at high voltage.** **a**, Differential conductance (d*I*/d*V*) as a function of voltage and temperature for 1D zigzag arrays with varied lengths. Gray areas indicate unmeasured regions in which the current level would be higher than the upper compliance of current (~20 nA) set for the protection of the devices. **b**, Threshold voltage as a function of temperature for the three devices in **(a)**. Inset: extrapolated threshold voltage at 0 K, as a function of length.

A linear $V_t$-$L$ dependence is observed for 1D zigzag QD arrays (Supplementary Fig. 4), similar to what is found in 1D linear arrays. A pronounced sublinearity at high temperature and low bias is also observed, similar to what is found in 1D linear arrays.

## E. Magnetoresistance response of the QD arrays

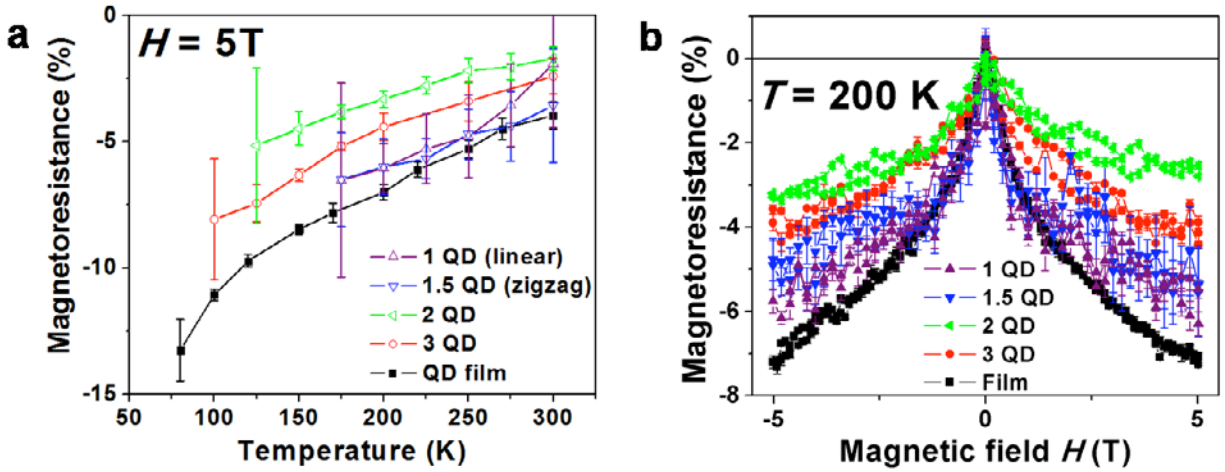


**Supplementary Figure 5. Magnetoresistance response of the QD arrays. a**, Magnetoresistance at an applied magnetic field of 5 T, as a function of temperature. **b**, Magnetoresistance at 200 K, as a function of applied magnetic field. Magnetoresistance is defined by the percentage change of resistance when an external magnetic field is applied. The number of QDs across the width of each array is label in the graph. 1D zigzag arrays are labeled as 1.5 QD.

We have measured the magnetoresistance (MR) response of all magnetite QD arrays investigated in this study. MR is defined by the percentage change of resistance when an external magnetic field is applied. Large negative MR is found for all devices (Supplementary Fig. 5), and similar temperature trends are found for all devices. This verifies that the electrical properties measured in our experiments arise from the magnetite QD arrays, since positive and much smaller MR is expected for conductance through non-magnetic materials. Reduced MR is found for quasi-1D and 1D arrays comparing to the QD film, possibly due to surface effects[33,34].

DOI: 10.1038/NNANO.2009.81

## F. Computer simulation of the bond percolation threshold for 2-QD-wide quasi-1D arrays

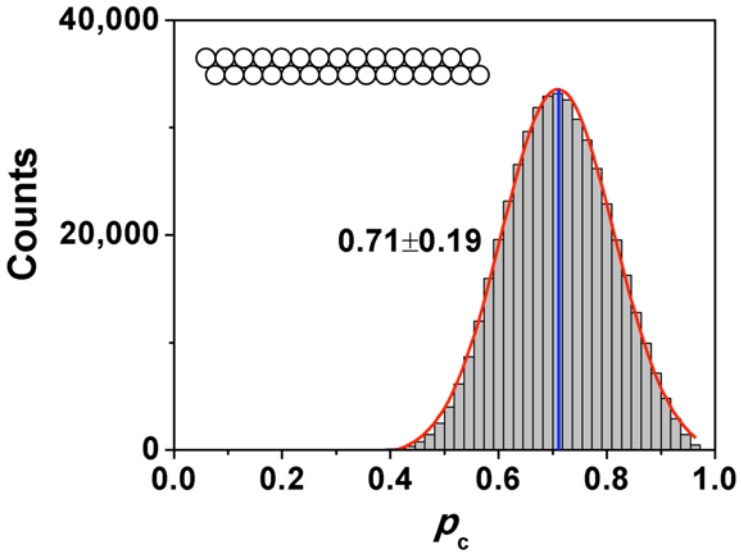


**Supplementary Figure 6. Computer simulation results of the bond percolation threshold for 2-QD-wide quasi-1D arrays.** Inset: the model system used for the simulation.

Computer simulation was carried out to calculate the bond percolation threshold, $p_c$, for 2-QD-wide quasi-1D arrays. The model system was a 2-QD-wide quasi-1D array 15 QDs in length, arranged in a close-packed triangle lattice (Supplementary Fig. 6 inset), similar to those investigated in our experiment. A Monte-Carlo method was used to randomly add in connecting bonds between neighboring sites, until a fully connected pathway was formed from the left end of the array to the right end. $p_c$ was then calculated as the number of connecting bonds used divided by the number of all possible bonds[35]. ~500,000 rounds of simulation were carried out, and the resultant distribution of $p_c$ is plotted in Supplementary Fig. 6, yeilding $p_c = 0.71 \pm 0.19$ (95% confidence).

## G. Optimization of the dip-coating speed

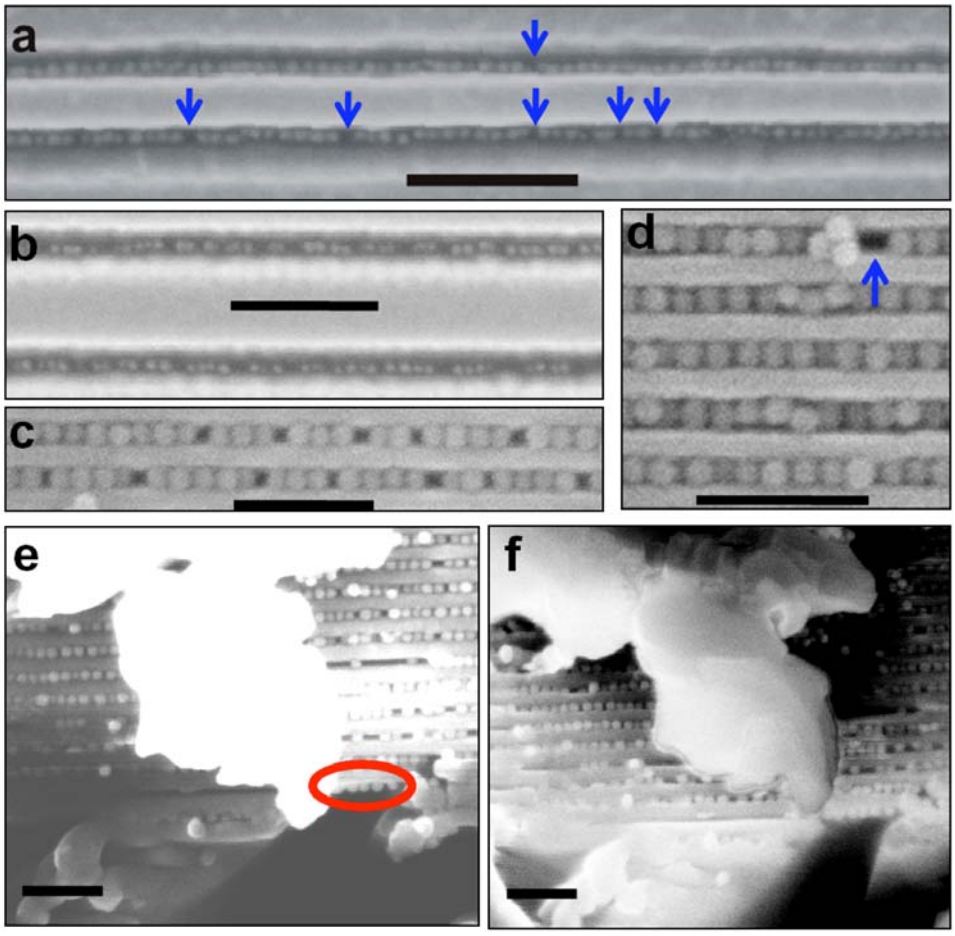


**Supplementary Figure 7.** SEM images for (a) *d* ~5 nm Au QDs assembled in ~50 nm deep trenches at a dip-coating speed that is slightly higher than the optimal speed. Blue arrows point to missing particles. (b) *d* ~5 nm Au QDs assembled at a still higher dip-coating speed. (c) 15 nm magnetite QDs assembled at a dip-coating speed that is slightly higher than the optimal speed. (d) 15 nm magnetite QDs assembled at the optimized speed. Blue arrow points to a defect (missing particle). (e) The red circle marks a 1D array of 15 nm magnetite QDs with the nanowire in front removed, imaged from the top. (f) The same sample imaged with 30$^{o}$ tilting.

In our experiments, we have noticed that the number of layers inside each nanotrench can be controlled by adjusting the concentration of the QD solution and the dip-coating speed. For example, for the 1D assembly of *d*~5 nm Au QDs, when the number of layers inside each nanotrench was controlled to be slightly below 1, defects were observed as missing particles in

DOI: 10.1038/NNANO.2009.81

the arrays (blue arrows in Suppl. Fig. 7a). When a higher dip-coating speed was used, the QD coverage was further reduced, and the submonolayer coverage resulted in discontinued QD 1D lines inside the nanotrenches (Suppl. Fig. 7b).

For all the QD arrays fabricated for electrical measurements, the QD concentration and dip-coating speed were carefully optimized to keep the number of layers inside each nanotrench to be as close to 1 as possible. We typically begin with higher dip-coating speeds, at which clear submonolayers of QDs form in the nanotrenches (Suppl. Fig. 7c). We then gradually reduce and optimize the dip-coating speed to achieve close-packed monolayers inside each nanotrench. Once optimized, the speed is stable and can be applied to multiple SNAP nanotrench arrays. For QD arrays assembled at the optimized speed, sparse defects (missing particles) indicate that there are no additional QDs beneath the QD arrays (Suppl. Fig. 7d). As noted in the main text, however, these sparse defects are not expected to affect our measurements, due to the large number of parallel channels.

Suppl. Fig. 7e,f show the SEM images of a 1D array of QDs (marked by the red circle in Suppl. Fig. 7e), after the nanowire in front was removed. This was achieved by scratching the sample with a diamond scriber. The side view image taken after the sample is tilted (Suppl. Fig. 7f) clearly demonstrates that there are no underlying QD layers (−note how the structures underneath the large flake on the top are revealed after tilting, so underlying QD layers should be observable if they do exist), and also that the QDs are approximately at the same height, thus align linearly in the trench. Granted, this is a somewhat perturbed sample, but the breaking of the wafer should, if anything, result in increased disorder for the QD arrays, and so we believe that this measurement is valid.

## References for Supplementary Information

33. Jang, S. J., Kong, W. J. & Zeng, H. Magnetotransport in $Fe_3O_4$ nanoparticle arrays dominated by noncollinear surface spins. *Phys. Rev. B* **76,** 212403 (2007).

34. Batlle, X. & Labarta, A. Finite-size effects in fine particles: magnetic and transport properties. *J. Phys. D-Appl. Phys.* **35,** R15-R42 (2002).

35. Stauffer, D. & Aharony, A. *Introduction to Percolation Theory* (Taylor & Francis, London, 1994).